Palaeogeography, Palaeoclimatology, Palaeoecology 617 (2023) 111488

Contents lists available at ScienceDirect

Palaeogeography, Palaeoclimatology, Palaeoecology

journal homepage: www.elsevier.com/locate/palaeo

Coral growth over the past 550 years in the central South China Sea linked to monsoon- and seabird-induced nutrient stress

Yi Liu [a,*], Shichen Tao [b,d], Ruoyu Sun [a], Chen-Feng You [c], Tzu-Hao Wang [c], Thomas Felis [e], Wang Zheng [a], Shaobo Sun [a], Xiaodong Liu [f], Qi Shi [d], Jianxin Zhao [g], Kefu Yu [b,*]

[a] Institute of Surface-Earth System Science, School of Earth System Science, Tianjin University, Tianjin, China
[b] Coral Reef Research Center of China; Guangxi Laboratory on the Study of Coral Reefs in the South China Sea; School of Marine Sciences, Guangxi University, Nanning, China
[c] Department of Earth Sciences, National Cheng Kung University, Tainan, Taiwan
[d] South China Sea Institute of Oceanology, Chinese Academy of Sciences, Guangzhou, China
[e] MARUM - Center for Marine Environmental Sciences, University of Bremen, Bremen, Germany
[f] School of Earth and Space Sciences, University of Science and Technology of China, Hefei, China
[g] Radiogenic Isotope Facility, School of Earth and Environmental Sciences, University of Queensland, St Lucia, Queensland, Australia

ARTICLE INFO

Editor: Hongqiang Yang

Keywords:
Boron isotopes
Coral biomineralization
Excess nutrient
Calcifying fluid
South China Sea
Porites

ABSTRACT

Nutrient enrichment is a widely recognized threat to coastal coral reefs. Yet its impact on open ocean reefs is largely unknown due to the lack of long-term observations at remote sites and the entanglement of various environmental factors affecting coral growth. Here we determined growth rates and the carbonate chemistry of calcifying fluid (CF) of massive corals over the last 550 years at a remote South China Sea reef ecosystem. We show that large growth variations cannot be fully explained by changes in seawater pH or temperature due to the antiphase relationship between growth rate and pH_{cf} as well as small sea surface temperature variations before the 1960s. Instead, coral growth rate decreases proportionally with past seabird populations over the past centuries. We suggest that excess nutrient loads through monsoon pumping and seabird migration played an important role in controlling coral growth at this remote reef ecosystem. Specifically, episodic eutrophication as indicated by a ~ 3 per mil increase in coral $\delta^{13}C$ has depressed coral growth by ~30% during 15th to 18th centuries, which is comparable to the modern decline. Thus, accurate projections of future coral growth for remote reefs under ongoing human activities and climate change needs to take into account the history of past nutrient inputs into these ecosystems under pre-anthropogenic conditions, which has been overlooked previously due to a lack of historical observations.

1. Introduction

Coral reefs in the tropical and subtropical oceans sustain the world's most diverse marine ecosystem. The formation of coral reefs fundamentally depends on fast calcification of coral skeletons. In recent decades, various reef sites (e.g. Great Barrier Reef, Red Sea, Caribbean Sea and South China Sea) exhibited dramatic declines in coral growth rates (Cantin et al., 2010; De'ath et al., 2009; Kang et al., 2021), threating reef-associated ecosystem functions, fisheries, tourism and coastal protection (Perry et al., 2018). Although such a widespread decline in coral calcification has been intensively studied, the primary responsible factors and their relative importance remain under hot debate (Hughes et al., 2017).

Rise in nutrient enrichment is rapidly emerging as one of the most potent threats to coastal coral reefs (Burke et al., 2002; Cybulski et al., 2020). Excess nutrients can lead to a growth decrease and even mass mortality of corals via increasing bioerosion, disease, competition from macroalgae and the susceptibility to thermal bleaching (Cunning and Baker, 2012; DeCarlo et al., 2020; Hallock and Schlager, 1986; Thurber et al., 2014). In contrast, open tropical oceans, typically oligotrophic, are thought to be devoid of excess nutrients. In the low-latitude oceans, distant from upwelling zones, surface seawater of the tropics and subtropics keeps low nutrient concentrations throughout the year because of the high insolation year round and well stratified upper waters (Tseng et al., 2005). Thus, previous studies have attributed the decrease of coral growth at open ocean sites almost exclusively to thermal stress and/or

* Corresponding authors.
E-mail addresses: liuyigeo@tju.edu.cn (Y. Liu), kefuyu@scsio.ac.cn (K. Yu).

https://doi.org/10.1016/j.palaeo.2023.111488
Received 24 December 2022; Received in revised form 24 February 2023; Accepted 27 February 2023
Available online 8 March 2023

ocean acidification (Albright et al., 2018; Hughes et al., 2017). However, fast-growing evidence indicates that large portions of the open oceans have already been significantly affected by anthropogenic nutrient input through atmospheric transport and deposition (Chen et al., 2019; Ren et al., 2017). For example, anthropogenic nitrogen can occupy about one quarter of the annual nitrogen input to the surface ocean in some regions (Ren et al., 2017). In addition, nutrient enrichments caused by seabirds' activities in a number of open ocean coral reefs from Hawaii, New Caledonia, Indian Ocean and South China Sea (SCS) have been recently reported (Graham et al., 2018; Lorrain et al., 2017; Wu et al., 2018a). The nutrient concentrations in coral reef seawaters at remote Pacific islands where abundant seabirds live are 10–100 times higher than that in surrounding seawater due to nutrients released from seabird guano (Lorrain et al., 2017). Yet, the effects of nutrients on the historical and current growth of corals in the open ocean are largely unknown, despite they play an important role in shaping coral growth in coastal oceans (Cybulski et al., 2020; Hallock and Schlager, 1986). This is mainly due to the lack of long-term data from remote locations and the difficulty to detangle the influence of nutrients from a variety of other environmental factors affecting coral growth.

New insights on coral calcification have been revealed recently by investigations of the micro-scale extracellular calcifying fluid (CF) from which corals precipitate their aragonitic skeleton at the calcification site (Allemand et al., 2011). The pH and the dissolved inorganic carbon (DIC) in the CF (pH_{cf} and DIC_{cf}), either directly measured by micro-sensors and fluorescent dyes (Guillermic et al., 2021; Sevilgen et al., 2019) or inferred from geochemical proxies [boron isotope ($\delta^{11}B$) and B/Ca ratio] (D'Olivo et al., 2019; McCulloch et al., 2017), are elevated by 0.3–0.6 units and a factor of ~2 relative to ambient seawater, respectively. The up-regulation of pH_{cf} is mainly achieved via enzymatic H^+ transport across the calicoblastic cell membrane, and the concentrating of DIC_{cf} is thought to be mediated through the diffusion of metabolic (respiration) carbon provided by the endosymbionts and/or through the bicarbonate anion transporters (*SLC4* family) within the coral host (Furla et al., 2000; Guo, 2019; Zoccola et al., 2015). Accordingly, the $[CO_3^{2-}]_{cf}$ and aragonite saturation state in the CF (Ω_{cf}, $\Omega = [Ca^{2+}]\ [CO_3^{2-}]_{cf}/K_{sp}$, where K_{sp} is the solubility product of aragonite) can be up to five times higher than the external seawater (Ω_{sw} = ~4), leading to more than one order of magnitude higher calcification rates than if precipitated directly from seawater (Mass et al., 2017). Field studies show that corals growing under environments of low Ω_{sw} such as submarine springs cannot sufficiently elevate their Ω_{cf} to a value that sustains growth rates similar to corals growing under ambient seawater conditions (Wall et al., 2019). Similarly, a CF record

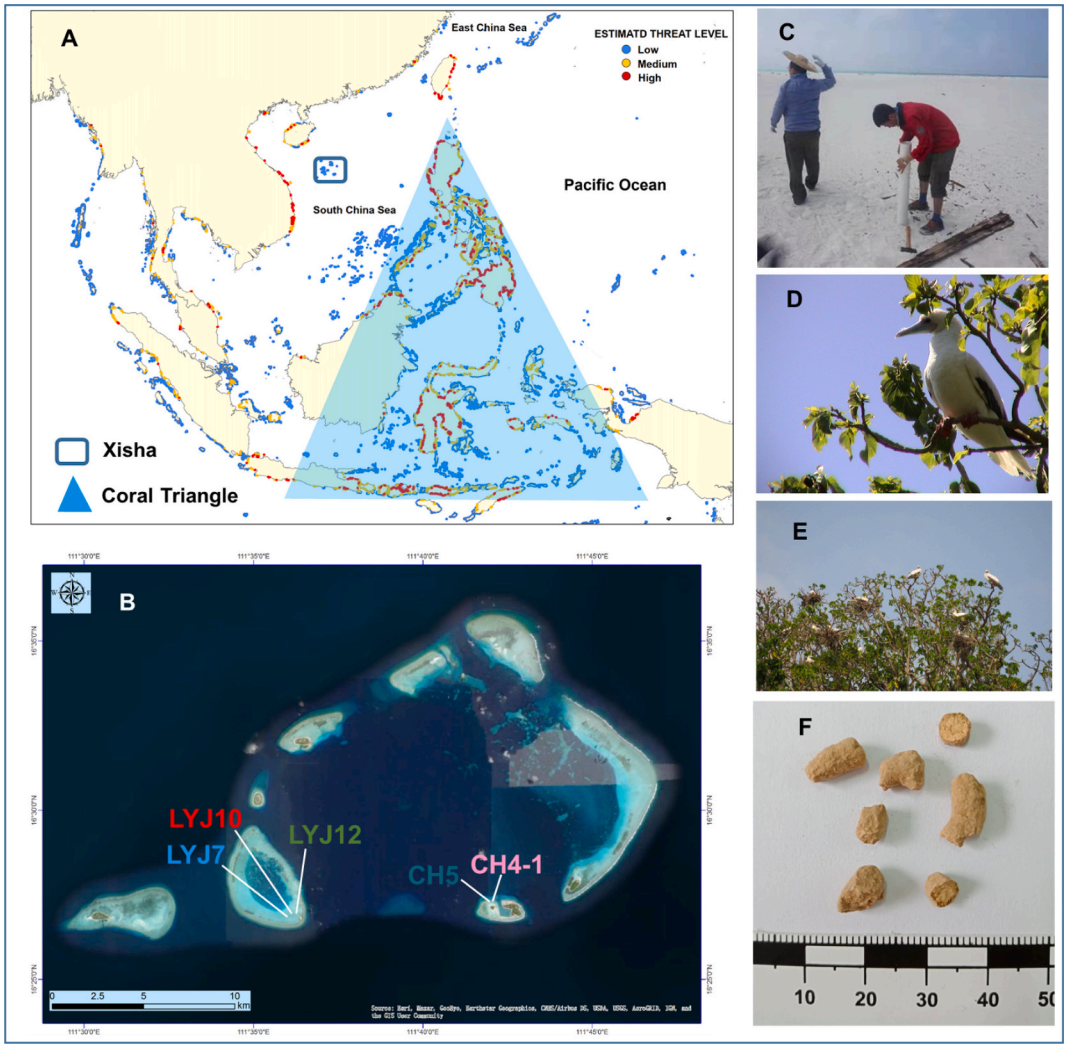

Fig. 1. Map of the study area. (A) Xisha Islands and their locations in the central SCS, about 600 km from the Coral Triangle. >600 reef-building coral species live in this region, threatened by sediment and nutrient loads (Burke et al., 2002). (B) Yongle Atoll, the western part of Xisha Islands, from which fossil coral cores (CH5, CH4–1, LYJ-7, LYJ-10 and LYJ-12) were drilled. (C) Close view of coral islands, which are covered by coral sands barely containing any nutrients. (D) and (E) Pictures of seabirds (red-footed booby, *Sula sula*) in the Xisha Islands. (F) Large numbers of guano pellets found in the sediments below shrubs. (For interpretation of the references to color in this figure legend, the reader is referred to the web version of this article.)

(1939–2013) retrieved from a coral off Australia revealed that ocean acidification (OA) has induced a long-term decrease in pH_{cf} and Ω_{cf}, which may account for the decline in coral calcification of the Great Barrier Reef (GBR) (D'Olivo et al., 2019). Moreover, the ability of corals to regulate CF chemistry could be impaired under thermal stress, resulting in a significant reduction in pH_{cf}, DIC_{cf} and calcification rate (Guillermic et al., 2021). Since the internal CF chemical parameters (i.e. pH_{cf}, DIC_{cf} and Ω_{cf}) play an important role in the coral calcification, their historical variations can help understanding roles of external environmental stress on coral calcification.

In this study, cores of six massive *Porites* corals from Xisha Islands (thereafter Xisha, 15°46′-17°08′N, 111°11′-112°54′E) in the central SCS (Fig. 1), which span the time interval from ~1450 to the 2000s, were recovered and analyzed for skeletal $\delta^{11}B$ and B/Ca (as proxies for pH_{cf} and DIC_{cf}) and growth rates. The unique oceanographic setting of this study site enables us to investigate nutrient effects on coral growth largely isolated from other environmental stressors. First, Xisha is a remote, pristine coral reef in the interior of the SCS far away (>300 km) from the continent, which is largely devoid of terrestrial input and direct human influence (at least before the 1960s). Second, distinctly different from the general pattern of the low-latitude ocean, the nutrient cycling in the open SCS exhibits large seasonal and interannual variations due to a shallow nutricline, monsoon-induced mixing and surface cooling (Liu et al., 2013; Tseng et al., 2005). Last, Xisha houses abundant seabirds (Fig. 1E) with >60 bird species (Wu et al., 2018a), which can concentrate marine-derived nutrients into the adjacent coral reef. Therefore, century-long coral proxy records from this site provide unique insights into the natural variability of coral growth in the open ocean, and its relation with past climate change as well as nutrient stress. This in turn will help to distinguish between anthropogenic and natural forcing of present changes in coral calcification rates and to develop strategies for coral reef management at open ocean sites.

2. Methods

2.1. Study sites and cores

The SCS is a large semi-enclosed marginal sea situated between the Asian continent and the Pacific Ocean (Fig. 1), which is strongly influenced by the intertropical convergence zone (ITCZ) and the East Asian monsoon (Yan et al., 2015). During boreal summer, the ITCZ migrates north and the warm and wet southwest monsoon prevails in this region (Yan et al., 2015). During winter, the ITCZ migrates south and the northeast winter monsoon prevails, which brings in cold and dry continental air from the Siberian and Mongolian highs. Xisha are a remote group of coral reefs in the central SCS, which are divided into two atolls: the Xuande Atoll and Yongle Atoll. Wide, deep channels connect the atolls' waters with the open ocean. Monthly SSTs range from ~25 to 30 °C. The surface salinity in Xisha ranges from 33.3‰ in October to 33.9‰ in February, with a mean value of 33.6‰. Xisha once provided habitats for over 60 bird species during the 1970s and abundant seabirds roosted in these islands (Xu et al., 2016). Most of the birds have disappeared on almost all of the islands at present, except the Dongdao Island which is now hosting >35,000 pairs of birds (Wu et al., 2018a). Some colonies have been greatly reduced in size, or even eliminated (Xu et al., 2016). It was estimated that the current population size of some species was only 10% of their historical level (Xu et al., 2016).

Coral cores (CH5, CH4–1, LYJ-7, LYJ-10 and LYJ-12) were drilled from five large, intact fossil corals (*Porites*) at the reef flat of Yongle Atoll and one modern live *Porites* coral (YXN-1) at the reef flat of Xuande Atoll. The 6 coral cores were cut into 7 mm-thick, 5 cm-wide slabs along the major growth axis with a high-speed diamond saw. Slabs were sectioned, washed with ultrapure water, and then dried for X-ray images (supplementary Fig. 1). We calculated annual growth rates for YXN-1 using the age-models developed from sub-annual resolution coral $\delta^{18}O$ results (Han et al., 2019a). For the other five cores, annual growth rates were measured across intervals of sub-parallel annual banding from X-ray images, because these cores had clear annual density band pairs. Along the main growth axis of the corals, the middle position of the white strip on the positive images of the slabs were set as the start and end baseline (winter–winter) of the annual growth, and we used the measurement tool of Photoshop software to measure the growth rate. Microstructures and mineral components of coral cores were examined using a field emission scanning electron microscope as well as X-ray diffraction analyses taken at ~50 cm intervals from the core tops. This testing for diagenetic alteration revealed that the cores were well preserved.

2.2. Elemental and Isotope ratio analysis

Subsamples (~15 mg) were milled in continuous 5-year intervals along the maximum growth axis and ground into homogeneous powder using a pre-cleaned agate. Subsamples were cleaned in Class 10 laminar flow benches at the Class 1000 clean room of the Isotope Geochemistry Laboratory (IGL), National Cheng Kung University, Taiwan. Coral powder was soaked overnight in deionized water, and then the supernatant was removed. Samples were washed five times by vigorously rinsing in deionized water, sonicating, and centrifuging (8000 rpm, 10 min). Organic matter was removed by soaking samples in 10% NaOCl and then rinsed, sonicated, and centrifuged for additional 5 times. The cleaned sample was split for B/Ca, B and C isotope measurements.

For B isotope measurements, the cleaned coral powder was fully dissolved in 100 μL of 1 M HNO_3. Purification of samples by microsublimation was performed following the methods in Wang et al. (2010), and then diluted to 20 ppb B. $\delta^{11}B$ measurements were made on a Thermo Fisher Scientific Neptune inductively coupled plasma mass spectrometer at IGL. Samples were bracketed with NIST SRM 951 to correct for mass bias, and long-term precision of the analysis was ±0.27‰ (2SD). Boron isotopic ratios are expressed using delta (δ) notations relative to the NIST SRM 951. At each analytical sequence, JCp-1 carbonate standard (*Porites* sp., Geological Survey of Japan) and one in-house standard Alfa-B (B ICP-MS solution, Alfa Aesar) were used to monitor analytical accuracy. The JCp-1 standard yielded a mean value of 24.20 ± 0.24‰ (2SD, $n = 9$).

For B/Ca ratio measurements, subsamples were dissolved in 3% HNO_3 to obtain solutions with a Ca concentration of 120 ppm and then analyzed on an Elan DRCI Quadrupole ICP-MS at the CAS Key Laboratory of Crust-Mantle and Environments, University of Science and Technology of China (USTC), Hefei. The JCp-1 standard yielded a mean value of 0.444 ± 0.030 mmol/mol (2SD, $n = 8$), which were consistent with a previously reported value (0.466 ± 0.014 mmol/mol, Chen et al., 2021).

The $\delta^{13}C$ measurements were carried out using an isotope ratio mass spectrometer MAT-253 in South China Sea Institute of Oceanology, Chinese Academy of Sciences. Results are expressed using delta (δ) notation relative to the Vienna Pee-Dee Belemnite (V-PDB) standard. Repeated analyses of the international standard NBS-18 showed a standard deviation of <0.05 ‰ ($n = 15$) for $\delta^{13}C$.

2.3. Carbonate chemistry of CF reconstructing

Several assumptions are made in reconstructing the CF chemistry from $\delta^{11}B$ and B/Ca, which has already thoroughly explored in numerous studies (see Guillermic et al., 2021, for a review) and hence are not elaborated further in this paper. $B(OH)_{4-}$ is the primary form of boron incorporated into coral skeleton and the concentration and $\delta^{11}B$ of total boron in the CF is the same as of the ambient seawater.

Briefly, The pH_{cf} was converted by boron isotope systematics based on the following equation (Zeebe et al., 2001):

$$pH_{cf} = pK_B - log\{[\delta^{11}B_{sw} - \delta^{11}B_{coral}] / [\alpha_{(B3-B4)}\delta^{11}B_{coral} - \delta^{11}B_{sw} + 1000(\alpha_{(B3-B4)} - 1)]\} \quad (1)$$

where $\delta^{11}B_{sw}$ and $\delta^{11}B_{coral}$ represent $\delta^{11}B$ in seawater [$\delta^{11}B_{sw}$ = 39.61 ‰ (Foster et al., 2010)] and coral, respectively, and $\alpha_{(B3-B4)}$ = 1.0272 (Klochko et al., 2006). The average of instrumental SST and SSS (1961–1996) at Xisha is 27.2 °C and 33.6 ‰. The dissociation constant of boric acid pK_B is 8.580 at 27.2 °C and a salinity of 33.6 (Dickson, 1990a). The external uncertainty of ±0.27‰ (2SD) for $\delta^{11}B$ data corresponds to a precision of better than ±0.02 units for pH_{cf}. All pH values are expressed on the total scale (pH_T).

The $[CO_3^{2-}]_{cf}$ was calculated by B/Ca ratios based on the following equation (McCulloch et al., 2017):

$$\left[CO_3^{2-}\right]_{cf} = \left[B(OH)_4^-\right]_{cf} K_D \Big/ [B/Ca]_{coral} \quad (2)$$

where $[B(OH)_4^-]_{cf}$ is the concentration of borate in the calcifying fluid, K_D is the molar distribution coefficient for boron in aragonite, and $[B/Ca]_{coral}$ is the molar ratio of boron to calcium in the coral skeleton. To estimate $[B(OH)_4^-]_{cf}$, we assume that the concentration of total inorganic boron in the calcifying fluid is the same as of the ambient seawater. The relative amounts of $B(OH)_4^-$ are derived from the pH_{cf}, determined from the $\delta^{11}B_{coral}$ isotopic measurements (see Eq. (1)). The K_D is calculated as a function of $[H^+]_{cf}$ based on the following equation (Holcomb et al., 2016):

$$K_D = 0.00297 \exp\left(-0.0202\,[H^+]_{cf}\right) \quad (3)$$

where $[H^+]_{cf}$ in the calcifying fluid is estimated from the coral $\delta^{11}B$-derived pH_{cf}.

The concentration of DIC_{cf} within the calcifying fluid is then calculated from pH_{cf} (eq. 1) and $[CO_3^{2-}]_{cf}$ (eq. 2) using the programme CO_2SYS provided by Lewis and Wallace (1998), with the carbonate species dissociation constants from Mehrbach et al. (1973) refined by Dickson and Millero (1987), the borate and sulfate dissociation constants from Dickson (1990a, 1990b), and the aragonite solubility constants from Mucci (1983).

Finally, aragonite saturation state of the CF (Ω_{cf}) is estimated from $[Ca^{2+}]_{cf}$ and $[CO_3^{2-}]_{cf}$ (from $\delta^{11}B$ and B/Ca). $[Ca^{2+}]_{cf}$ is assumed equal to that of the ambient seawater (McCulloch et al., 2017).

Uncertainties on the estimates of DIC_{cf} and $[CO_3^{2-}]_{cf}$ were calculated by using Monte-Carlo simulations that randomly used values of the determined parameters ($\delta^{11}B$ and B/Ca) between the mean ± SD ($\delta^{11}B$ SD = 0.14‰ and B/Ca SD = 0.015 mmol/mol) over 1000 iterations.

Given the annual-mean SSTs (~2 °C) variability of the SCS over the last 1 ka (Yan et al., 2015; Deng et al., 2017), variations of calculated pH_{cf}, DIC_{cf}, $[CO_3^{2-}]_{cf}$ and Ω_{cf} value due to thermodynamic effects of SST changes were all negligible (Mehrbach et al., 1973; Mucci, 1983; Dickson and Millero, 1987; Dickson, 1990b). Thus in our pH_{cf}, DIC_{cf} and Ω_{cf} reconstructions, we have not taken into account SST changes.

2.4. Dating

The fossil corals were dated by ^{230}Th techniques. Approximately 150 mg from each coral slab were prepared and weighted at the Radiogenic Isotope Facility (RIF), School of Earth and Environmental Sciences, University of Queensland, Australia. U—Th isotopic ratio measurements were performed on a multi-collector inductively coupled plasma mass spectrometry (MC-ICP-MS) following the analytical protocol described by Clark et al. (2014a, 2014b). The chronology of each coral was then established by counting the annual bands backward and forwards from the dated calendar year. All the time series are plotted on the original ^{230}Th dates except LYJ7. A better match in overlapping intervals of the LYJ7 and LYJ10 CF records occurs when the ^{230}Th date of LYJ7 is shifted, within dating error, towards 5 years older. The annual growth of the same subsamples supports the adjusted age model for LYJ7 (Fig. 2A).

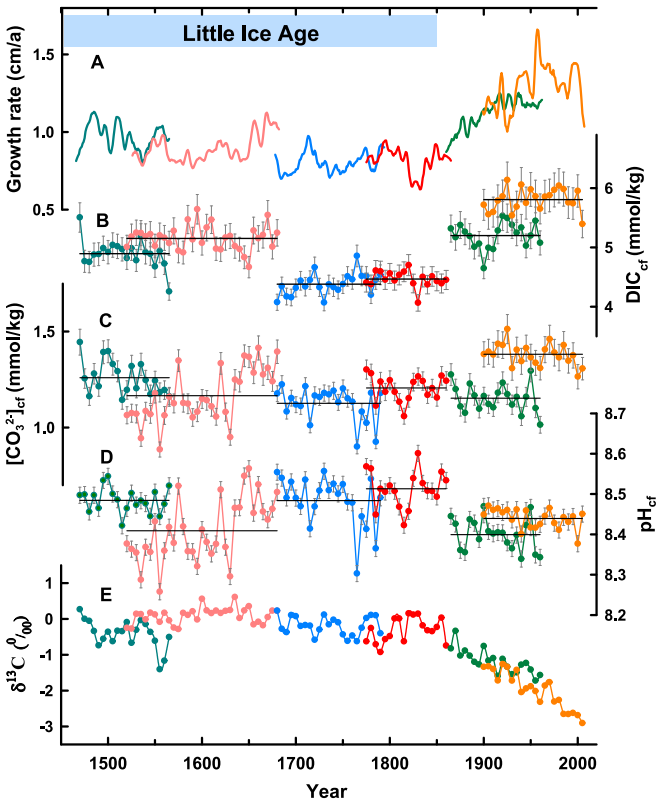

Fig. 2. Time series of coral growth rates and CF chemistry over the past 550 years. (A) Annual growth rate (five-point running means). The growth rates were smoothed with 5-point running means to minimize the impact of dating errors and disorders in annual density bands (Lough and Barnes, 1997). (B) to (D) DIC_{cf}, $[CO_3^{2-}]_{cf}$ and pH_{cf}. (E) Coral $\delta^{13}C$. Error bars in (B) and (C) represent ±1 standard deviations (1SD), while error bars in (D) represent ±2 SD. The horizontal lines in (B) to (D) indicate the average values of CF chemistry for each colony.

2.5. General circulation modeling

The outputs from the Last Millennium experiment conducted with the Community Climate System Model 4 (Landrum et al., 2013), which covers the years of 850–1850 CE, are employed in this study. The Last Millennium experiment was designed under the framework of Paleoclimate Model Intercomparison Project 3. The horizontal resolution for the modeling data is approximately 1.25° × 0.90°. To examine the response of the climate system to external forcing in the modeling experiment, two typical periods (1151–1100 CE and 1651–1700 CE) were chosen as Medieval Warm Period (MWP, ~950–1250 CE) and Little Ice Age (LIA, ~1450–1850 CE) (Mann et al., 2009; Masson-Delmotte et al., 2014; Neukom et al., 2019), respectively, based on the simulated averaged temperature over the NH. The wind vector and sea surface temperatures during January were calculated.

3. Results

The chronologies of cores drilled from the five fossil corals (CH5, CH4–1, LYJ-7, LYJ-10 and LYJ-12) were established by combining U—Th dating and the counting of annual density-band pairs. The chronology for the modern coral (YXN-1) was established by the counting of annual density-band pairs and the known year of core recovery when this colony was still alive (Data S1). The time intervals of the five fossil and one modern coral records range from 90 to 165 years (CH5,1468–1567; CH4–1, 1518–1682; LYJ-7, 1678–1792; LYJ-10, 1773–1862; LYJ-12-21,863–1962; YXN-1, 1898–2007, Data S2), roughly extending from the LIA, to the modern era of anthropogenic

warming and ocean acidification.

The annual growth rates of these coral colonies ranged from 0.65 cm/yr to 1.77 cm/yr (Fig. 2A). The two most recent cores have an average growth rate of 1.23 ± 0.22 cm/yr in the 20th century, which is similar to two previously reported Xisha *Porites* corals (1.16 ± 0.37 cm/yr and 1.10 ± 0.22 cm/yr, Table 1) for the same period (Kang et al., 2021; Yan et al., 2019). The average growth rate of four colonies living in the LIA is 0.87 ± 0.11 cm/yr, which is significantly (*t*-test, $p < 0.0001$) lower than the colonies in the 20th century. Coral $\delta^{13}C$ values were relatively high before ~1850s and showed a pronounced decrease from ~0 ‰ to −3 ‰ afterwards (Fig. 2E).

Considerable variability in reconstructed, coral-based pH_{cf}, DIC_{cf} and $[CO_3^{2-}]_{cf}$ are observed within decadal to centennial time windows (Fig. 2B, C, D). The variation ranges for pH_{cf}, DIC_{cf} and $[CO_3^{2-}]_{cf}$ are from 8.26 ± 0.02 to 8.60 ± 0.02, 4064 ± 138 to 6134 ± 303 umol/kg and 887 ± 39 to 1514 ± 76 umol/kg, respectively. The values of these CF chemical parameters were significantly elevated relative to seawater but are largely within the reported ranges of *Porites* corals (pH_{cf}: ~8.25 to 8.71; DIC_{cf}: ~3100 to 6200 umol/kg, Chen et al., 2021; D'Olivo et al., 2019; McCulloch et al., 2017). Moreover, large intercolony offsets were observed, especially for DIC_{cf} with a mean offset as high as 1425 μmol/kg.

4. Discussion

Similar large intercolony offsets of CF carbonate chemistry have been observed in previous studies (Chen et al., 2021; D'Olivo et al., 2015). The exact causes behind these differences are not clear, but they likely reflect variability in individual physiological parameters of the corals (e.g., species or gender related) or local environmental conditions (e.g., light regime) (D'Olivo et al., 2015). Our following discussion will mainly focus on the relative changes instead of absolute values, and thus the temporal trends and patterns of CF chemistry will be largely unaffected.

4.1. Temperature affects variability in DIC_{cf} but not pH_{cf}

Previous studies have shown that temperature can modulate the CF carbonate chemistry (McCulloch et al., 2017). Rising temperature can promote metabolic carbon production of zooxanthellae and increase $[DIC]_{cf}$, leading to enhanced abiotic kinetics of aragonite precipitation (D'Olivo et al., 2019). This would cause a decline in pH_{cf} as more protons are being produced through CO_2 influx and aragonite formation (Guo, 2019). Thus, an inverse seasonal fluctuation of the pH_{cf} and DIC_{cf} are typically displayed (McCulloch et al., 2017). Our observed inverse relationship between the pH_{cf} and DIC_{cf} variations (Fig. 2B, D) seems to be broadly consistent with this temperature-driven interactive dynamics of pH_{cf} and DIC_{cf} on a seasonal time, in particular during the pre-1900 CE period. Although high resolution and continuous SST records from the central SCS spanning the last 550 years are currently not available (Yan et al., 2015), a century-long annual coral Sr/Ca-based SST reconstruction from the northern SCS (Deng et al., 2017) exhibits similar temporal patterns to our CF record (supplementary Fig. 2). Applying the sensitivity of ~11% to 14% /°C of *Porites* DIC_{cf} to temperature obtained at the GBR (McCulloch et al., 2017) to our study, results in an amplitude of DIC_{cf} (~500–900 umol/kg) that can be largely explained by temperature change (~1–2 °C).

To evaluate the temperature contribution to our coral pH_{cf} records, we extracted the seawater pH(pH_{sw}) signal from pH_{cf} following the method developed by D'Olivo et al. (2019):

$$pH_{cf}\ \text{anomaly} = pH_{sw}\ \text{anomaly}^{*}0.46–0.02^{*}\text{T anomaly} \quad (4)$$

where 0.02 is the sensitivity of *Porites* pH_{cf} to temperature (~0.02 pH units /°C), and 1/0.46 is the sensitivity of *Porites* pH_{cf} to seawater pH_{sw} (McCulloch et al., 2012). Rearranging eq. (4) results in eq. (5) which allows pH_{sw} to be calculated from pH_{cf} and SST.

$$pH_{sw}\ \text{anomaly} = \left(pH_{cf}\ \text{anomaly} + 0.02^{*}\text{T anomaly}\right)/0.46 \quad (5)$$

Three temperature scenarios were tested: Constant SST, annual SST from the northern SCS (Deng et al., 2017) and random SST [normally distributed with mean ± 1SD matching the instrumental SST (0.43 °C) or SST reconstruction (0.72–1.1 °C, here 1.1 °C was used)]. We find no significant differences in pH_{sw} amplitude in all three scenarios (Fig. 3) and the pH_{sw} pattern was the same as the pH_{cf} in each scenario. Thus, given the low sensitivity of *Porites* pH_{cf} to temperature and the limited variations in instrumental (supplementary Fig. 3) or reconstructed annual SST (Deng et al., 2017) compared to seasonal SST, temperature is unlikely to be the main driver of pH_{cf} on longer time scales at our study site.

It has been suggested that sporadic subdecadal intervals of anomalously low pH_{cf} may be related to thermal bleaching of corals (Wei et al., 2009). However, thermal bleaching of our samples can be largely excluded given that most of low pH_{cf} values occurred during the LIA (Masson-Delmotte et al., 2014), which although not being a globally coherent cold period (Neukom et al., 2019), likely did not favour extreme thermal events as observed in the modern era of rapid global warming. A coral Sr/Ca-based reconstruction suggests ~1 °C lower SST at Xisha during the LIA compared to the 20th century (Yan et al., 2015). Moreover, thermal bleaching usually causes an anomalous reduction in coral growth rate and negative drifts in $\delta^{13}C$ (Wei et al., 2009), which both were not observed in our time intervals with anomalously low pH_{cf}.

4.2. Reef-water pH_{sw} modified by monsoon controls pH_{cf} and $[CO_3^{2-}]_{cf}$

The coral pH_{cf} record could be interpreted as showing a slight decrease towards the Industrial Era, a potential trend that is accompanied by a negative drift of $\delta^{13}C$ values (Fig. 2D, E). This is consistent with previous coral $\delta^{11}B$-pH studies from Xisha (Kang et al., 2021) and elsewhere such as the GBR (D'Olivo et al., 2019) and South Pacific (Wu et al., 2018b), suggesting that OA may cause a long-term reduction in pH_{cf}. However, anthropogenic CO_2 can only induce a ~ 0.1 pH unit drop in pH_{sw}, which translates into about 0.05 units of pH_{cf} variation (McCulloch et al., 2012). The observed large variability of 0.1–0.2 pH_{cf} must be linked to other mechanisms. Given the present-day small variation in surface-ocean pH_{sw} throughout the SCS (< 0.05 pH units; supplementary Fig. 4), any contribution by changes in surface currents or the redistribution of water masses were also considered to be minor.

Reef-water pH_{sw} is known to change substantially during a day, between seasons, and on longer timescales (DeCarlo et al., 2017; Liu et al., 2014; Pelejero et al., 2005), due to biogeochemical and local physical processes such as calcification, respiration, photosynthesis and exchange of reef waters with open seawaters. An ecological survey carried out in 2013 at the Yongle Atoll (Xisha) revealed a high abundance of benthic flora and fauna with a mean coral cover of 17% (Zhao et al., 2016). There, lagoon seawater pCO_2 displayed a large diurnal cycle, ranging from ~240 to 863 μatm (Yan et al., 2018). Indeed, at the Dongsha Atoll, a reef in the northeastern SCS similar to Yongle Atoll, diurnal pH_{sw} changes of up to 1.2 pH units were observed (DeCarlo et al., 2017), which was attributed to the high abundance of calcifiers

Table 1
Summary of *Porites* growth rates at Xisha in SCS (cm/yr).

Time Interval	Mean	1SD	Median	Min	Max	N
20th century						
Ref. (Yan et al., 2019)	1.10	0.22	1.09	0.45	2.31	4
Ref. (Kang et al., 2021)	1.16	0.37	1.09	0.32	2.56	9
This study	1.23	0.22	1.17	0.82	1.77	2
LIA						
This study	0.87	0.11	0.87	0.65	1.13	4

Mean: average value; SD: standard derivation; Median: median value; Min: Minimum value; Max: Maximum value. N: number of coral colonies.

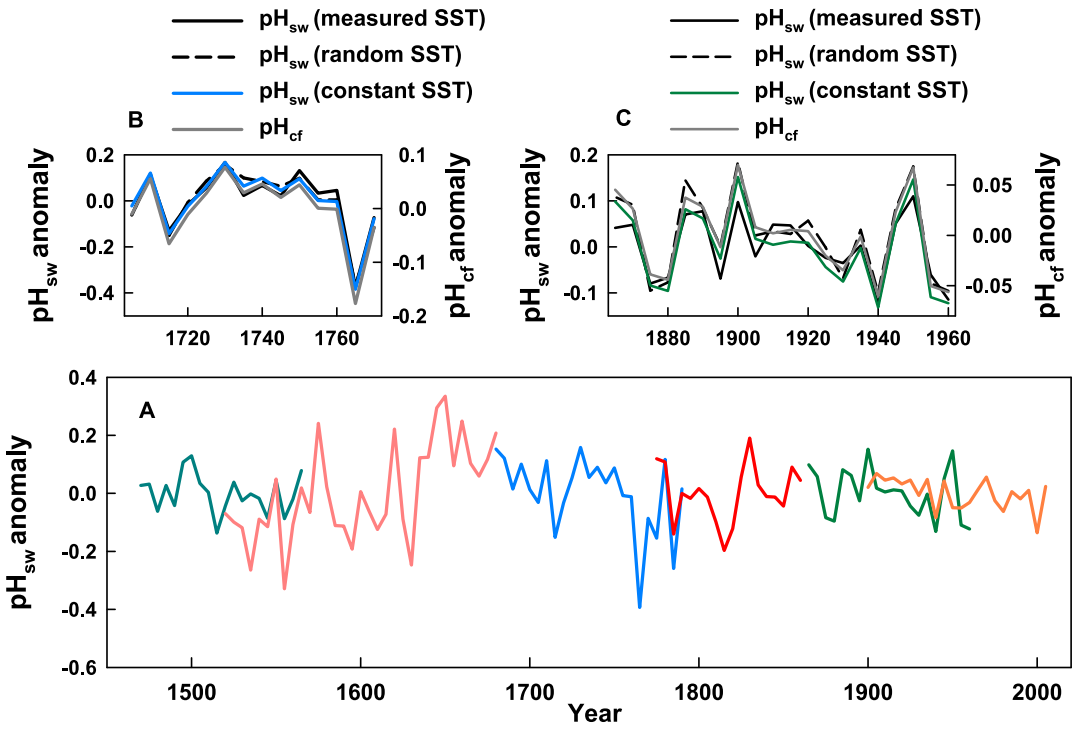

Fig. 3. Comparison between pH_{cf} and estimated pH_{sw} anomalies using different temperature scenarios. Estimated reef-water pH_{sw} anomalies using a constant SST (A). Estimated reef-water pH_{sw} using a constant SST, a random SST and reconstructed SST records from the Northern SCS for colony LYJ-7 (B) and for colony LYJ-12 (C). Reconstructed SST is from Deng et al. (2017) and random SST is normally distributed with mean ± 1SD (1.1 °C) matching SST reconstruction.

(coral) and primary producers (fleshy algae and seagrass) as well as the relatively shallow reef flat (1–3 m).

We suggest that the large variations in our coral pH_{cf} record from Xisha are likely linked to the chemical conditions in the semi-closed reef waters that are modified by the migration of ITCZ. When the ITCZ migrates north during boreal summer, the mild southwest monsoon carries warm and humid air into the SCS (supplementary Fig. 5). When the ITCZ migrates south during boreal winter, the East Asian winter monsoon (EAWM) prevails in the SCS, advecting cold and dry air from the continent (Yan et al., 2015). Monthly mean wind speed at the study site shows prominent peaks in the winter season, ranging from 2 to 11 m/s (supplementary Fig. 6). The annual wind speed is strongly correlated with the winter wind speed ($R^2 = 0.85$, $n = 9$, $p < 0.001$, supplementary Fig. 7), but not with the summer wind speed ($R^2 = 0.06$, $p = 0.53$). This indicates that changes of the annual wind speed depend largely on variations of the winter monsoon. Consequently, time intervals of stronger EAWM associated with a more southward position of the ITCZ (Yan et al., 2015) would enhance the mixing of reef waters with open seawaters (Liu et al., 2014), decreasing reef-water CO_2 that has been built up by the intense calcification activities of corals (DeCarlo et al., 2017). The opposite effect occurring during time intervals of a more northward position of the ITCZ would cause an accumulation of reef-water CO_2 and a decrease in reef-water pH_{sw}, which is in turn reflected in pH_{cf}.

Our proposed mechanism is supported by the migration of the ITCZ in the past as documented by various other monsoon records at the global scale (Haug et al., 2001; Schneider et al., 2014; Yancheva et al., 2007). Long-term meridional migration of the annual mean position of the ITCZ and the corresponding anti-phase behavior of the winter and summer monsoon intensity over the late Holocene in response to Northern Hemisphere (NH) warm-cold intervals have been widely demonstrated over low-latitude regions including the SCS (Deng et al., 2017; Yancheva et al., 2007). Migration of the annual mean position of the ITCZ provides a coherent explanation for the observed variability in both pH_{cf} and DIC_{cf} at Xisha over the past~550 years, as well as the antithetic relationship between them. Indeed, time intervals of a more southward displaced ITCZ as recorded in the Cariaco Ti record from tropical South America (Haug et al., 2001) are broadly consistent with high pH_{cf} and low DIC_{cf} values in the coral records, and vice versa (Fig. 4), though the dating errors (± ~30 yrs) of the Cariaco Ti record might influence our comparison presented here. This temporal coincidence could also be observed in the ITCZ migration based on instrumental data (Schneider et al., 2014) over the last century (supplementary Fig. 8). Moreover, we find a similar relationship in a previous coral pH_{cf} record (Kang et al., 2021) from Xisha (supplementary Fig. 9), corroborating our suggested mechanism. We note a higher $[CO_3^{2-}]_{cf}$ occurring during winter-like conditions, and $[CO_3^{2-}]_{cf}$ values in all the colonies that were significantly positively correlated with pH_{cf} (supplementary Fig. 10), but not with DIC_{cf}. This points to a more dominant role of pH_{cf} than DIC_{cf} in determining $[CO_3^{2-}]_{cf}$ variations within each colony.

4.3. Monsoon- and seabird-induced nutrient stress suppressed coral growth

Our records reveal that intervals of prominent southward shifts of the ITCZ generally coincide with intervals of slow growth rates of corals in the central SCS during the LIA, and vice versa (Fig. 4). We note that faster coral growth occurs during northward shifts of the ITCZ (weaker EAWM) despite lower Ω_{cf} (assuming a constant $[Ca^{2+}]_{cf}$, Supplementary Section S1), which is usually thought to result in unfavorable CF conditions for calcification. Aragonite precipitation is a temperature-dependent reaction and the increase in coral growth rate may simply reflect enhanced kinetics of abiotic aragonite precipitation at high temperature (Burton and Walter, 1987). The observed low average growth rates during the LIA can be explained by the ~1 °C lower SST at Xisha compared to the 20th century (Yan et al., 2015). Most of the ~1 °C rise in SST took place after the late 1970s (supplementary Fig. 3). However, 20th century growth rates apparently started to decrease after 1960 before this large increase in temperature (Fig. 5A), though

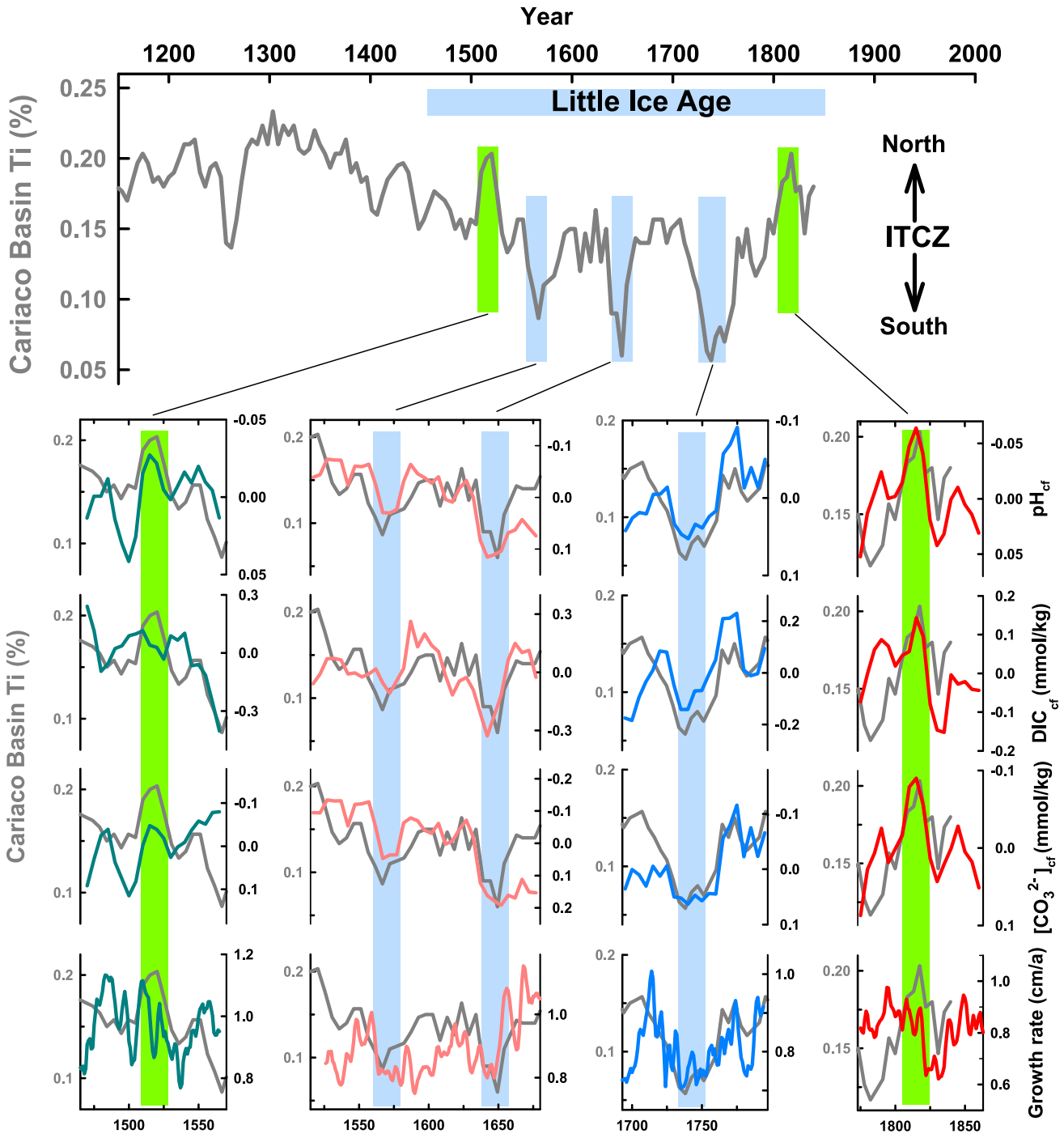

Fig. 4. Comparison of coral CF chemistry and growth rates with latitudinal ITCZ migration for the LIA. Ti content in Cariaco Basin sediments (gray lines) (Haug et al., 2001) reflect past ITCZ movements over tropical South America that have been frequently interpreted in a global context. The LIA is marked by an overall southward displacement of the ITCZ punctuated by notable multi-decadal ITCZ shifts to extreme southern (light blue bars) and northern positions (green bars). The pH_{cf}, DIC_{cf} and $[CO_3^{2-}]_{cf}$ anomalies are smoothed with 3-point running means (color lines). The annual growth rates are smoothed with 5-point running means (color lines). The colors for different coral colonies are the same as Fig. 1. The original Cariaco chronology (the calendar year of the B.P.) is converted to the A.D. year here. (For interpretation of the references to color in this figure legend, the reader is referred to the web version of this article.)

absolute growth rates were still higher than during the LIA. A similar decrease in growth rates since the 1960s was reported recently based on nine modern *Porites* colonies from the Xisha (Kang et al., 2021) (Fig. 5A). Further, the SST variations at the study site are too small (Han et al., 2019a) (1SD of the annually averaged SST was 0.43 °C) to induce such a large change in growth or calcification rate. Here, we use a bio-inorganic model (McCulloch et al., 2012) to estimate the effects of temperature and Ω_{cf} on aragonite precipitation kinetics. This calcification model is based on an empirical exponential rate dependence law for aragonite precipitation (Burton and Walter, 1987): $G = k(\Omega_{cf} - 1)^n$, where G is the modeled calcification rate of the coral, k is the rate constant [$k = 0.0024*(-0.0177*T^2 + 1.47*T + 14.9)$] and n is the order of the reaction ($n = 0.628*T + 0.0985$). The model calculation shows that aragonite precipitation rate increases by ~0.6 g cm^{-2} yr^{-1} (+34%) when Ω_{cf} increases from 18 to 21, but it decreases by only ~0.4 g cm^{-2} yr^{-1} (−24%) when T decreases from 27 to 26 °C. Therefore, contrary to the

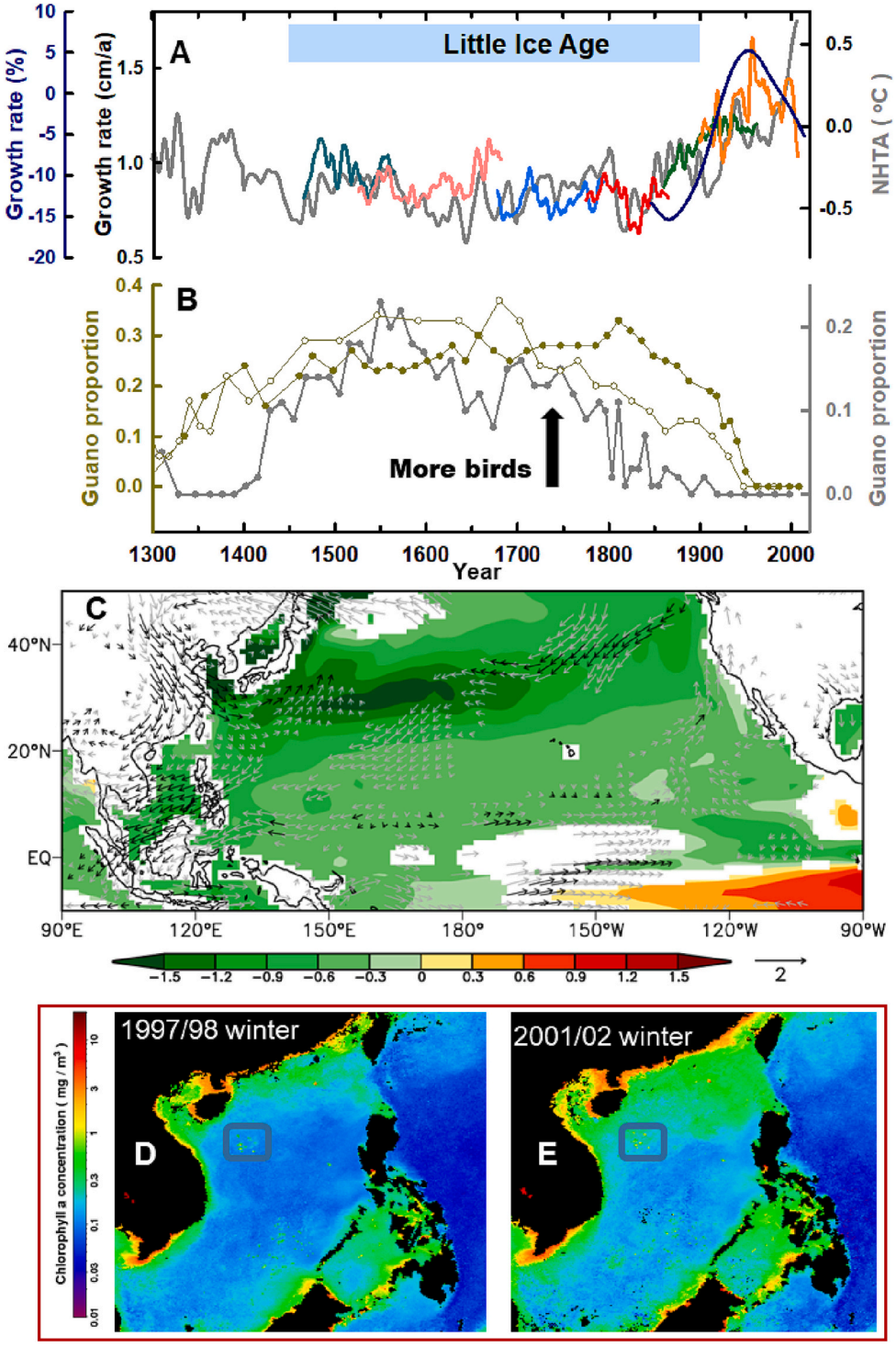

Fig. 5. Coral growth in response to the EAWM. (A) Annual growth rate (five-point running means, color lines) in this study, the percentage anomaly of growth rate (dark blue line) based on nine *Porites* colonies in a previous study (Kang et al., 2021) at Xisha and Northern Hemisphere temperature anomaly (NHTA, gray line) (Mann et al., 2009). (B) Past seabird population reconstruction from three separate reef islands in Xisha (Xu et al., 2016). (C) Differences in the 850 hPa wind vectors (m/s) and sea surface temperatures (SST, °C, shaded) during January between the LIA and MWP in the Last Millennium experiment by CCSM4[55]. Black vectors show the differences in both meridional and zonal winds significant at 99% confidence level and gray ones show those significant in either. Shading shows the significant SST differences at the 99% confidence level. Winter chlorophyll concentrations during weak EAWM (D) and strong EAWM (E) years (SeaWiFS level 3, http://oceancolor.gsfc.nasa.gov/). (For interpretation of the references to color in this figure legend, the reader is referred to the web version of this article.)

observed negative response of coral growth to the southward movement of ITCZ (stronger EAWM), the combined effect of lower temperature and higher Ω_{cf} results in an increase of calcification rate by ~0.2 g cm^{-2} yr^{-1} (+10%). This indicates that in addition to the reef-water pH_{sw} and temperature, other factors must also play an important role in coral growth at Xisha.

We suggest that nutrient input associated with the EAWM and migration of seabirds exerted an important control on the coral growth. The mixed-layer depth of the SCS is mainly controlled by the EAWM through wind-induced mixing and surface cooling (Tseng et al., 2005). When the mixed-layer depth is deeper than the depth of the nutricline top in winter, more nutrients are pumped into the oligotrophic surface waters in the open SCS waters as wind driven nutrient pumping is more efficient (Liu et al., 2013). Due to a shallower nutricline and steeper vertical nutrient gradient, the increase of surface Chl-α concentrations in the SCS is ~10 times higher compared to the northwestern Pacific under identical wind forcing (Liu et al., 2013). The nutrient-fueled blooms in the open SCS are reflected by a significantly expanded Chl-α (>0.5 mg m^{-3}) surface area in strong EAWM years (Fig. 5D and E), in contrast to weak EAWM years that are characterized by low Chl-α (<0.1 mg m^{-3}). There is indeed a significantly positive correlation between the wind speed and Chl-α concentrations (supplementary Fig. 11). Therefore, any

changes in past EAWM strength would have caused a large change in nutrient supply and, subsequently, in biological productivity. It is likely that seabirds feeding in the open ocean delivered and concentrated nutrients (N, P) in the form of guano on the reef islands where they roosted and breaded (Wu et al., 2018a). The importance of seabirds to deliver large quantities of marine-derived nutrients to coral reef ecosystems has been recently highlighted (Graham et al., 2018; Lorrain et al., 2017). Corals are highly adapted to nutrient deficient environments. Importantly, the large amount of nutrients brought into coral reef ecosystems can stimulate the increase in benthic fleshy algae and seagrass. However, these fast-growing organisms not only compete for space but also reduce water transparency (Hallock and Schlager, 1986), thereby suppressing coral growth (Fig. 6).

Our proposed mechanism is in line with the model simulations of the Last Millennium experiment conducted with the Community Climate System Model 4 (Landrum et al., 2013) and seabird population reconstructions for Xisha (Xu et al., 2016). The modeled northeast wind speed (winter monsoon) is significantly increased in the SCS during the LIA (Fig. 5C). The seabird population size from three reef islands of Xisha all peaked during the LIA as inferred from the guano proportion in the ornithogenic sediments (Fig. 5B). The population size of seabirds is a reflection of the zooplankton and prey richness in this oligotrophic ocean (Xu et al., 2016), which is determined by primary productivity driven by the EAWM. The large number of plants at present and large quantities of avian biological remains (e.g. guano, bones, eggshells) found in the ornithogenic sediments from the Xisha (supplementary Fig. 12) are testimony of seabird densities in the past. We note that the two series of guano proportion began to decline in ~1700–1750 and one series of guano proportion began to decline around 1800. The small time mismatch between guano proportion and growth rate maybe caused by dating errors (Xu et al., 2016).

Further support for the depressed coral growth linked to excess nutrient input during the LIA is provided by the corals $\delta^{13}C$ records. The observed ~3 per mil difference in $\delta^{13}C$ between LIA and modern corals is about two to three times higher than reported for corals in the Pacific Ocean and elsewhere (Pelejero et al., 2005; Swart et al., 2010; Wu et al., 2018b) (Fig. 7), and too large to be solely ascribed to the absorption of

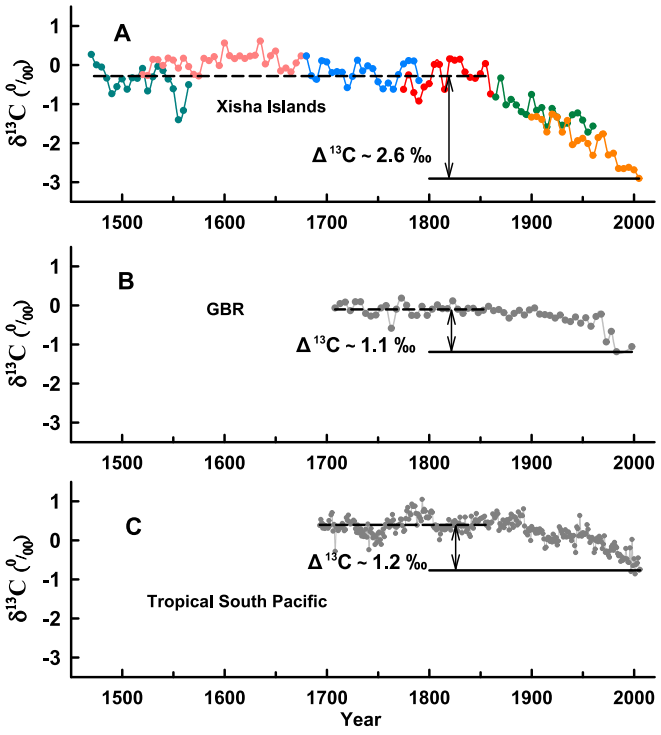

Fig. 7. Comparison of coral $\delta^{13}C$ in this study with Pacific coral records. (A) Xisha in this study, (B) Great Barrier Reef (GBR) (Pelejero et al., 2005) and (C) tropical South Pacific (Wu et al., 2018b). The average difference in coral $\delta^{13}C$ (~2.6 ‰) between the LIA (here, 1468–1855) and the minimum value in modern times (here, 2007) in Xisha is larger than reported for Pacific coral records, which is typically in the range of ~1–1.5‰ (Swart et al., 2010; Wu et al., 2018b). The latter is attributed to the Suess effect.

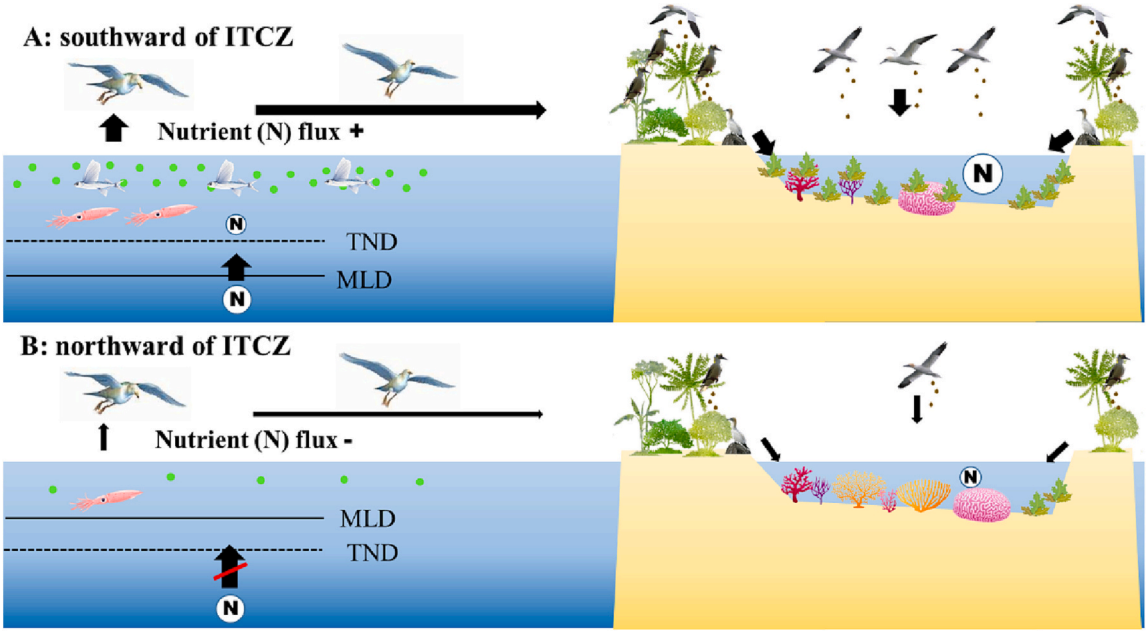

Fig. 6. Schematic illustration of the influence of the annual mean position of the ITCZ and seabirds on nutrient (i.e. N, P) input into the Xisha coral reef ecosystem. (A) During a more southward position of the ITCZ, the stronger winter monsoon drives a deeper mixed layer depth (MLD) than the depth at the top of the nutricline (TND), enabling more nutrients pumped into the surface ocean and thus to promote greater primary productivity and zooplankton biomass (Liu et al., 2013; Tseng et al., 2005). Seabirds concentrate these nutrients from the large marine area into the adjacent coral reef in the form of guano and stimulate fleshy algae bloom. The opposite scenario occurs during a more northward ITCZ position (B).

anthropogenic CO_2 (Suess effect). Given the insignificant correlations between $\delta^{13}C$ and growth rate before 1860 ($R^2 = -0.04$, $N = 94$, $p = 0.0713$), the variation of $\delta^{13}C$ was likely not caused by kinetic isotope effects related to growth rate (McConnaughey, 1989). High primary productivity is known to increase seawater DIC $\delta^{13}C$ via the preferential removal of seawater $^{12}CO_2$ during phytoplankton photosynthesis (Descolas-Gros and Fontugne, 1990). Thus, the large $\delta^{13}C$ variations (~0.5–1‰) likely reflect past dramatic productivity changes and episodic eutrophication in the Xisha reef waters. Indeed, after the ^{13}C Suess effect being removed, modern Xisha coral $\delta^{13}C$ records mainly reflect changes in primary productivity (Han et al., 2019b).

5. Conclusions

The growth and CF chemistry parameters of six massive *Porites* colonies from the central SCS show consistent responses to climatic oscillations over the past ~550 years, with lower DIC_{cf} and growth rates, and higher pH_{cf} and Ω_{cf} during southward shifts of the ITCZ and vice versa. The CF chemistry variability is driven by fluctuations of reef-water pH and temperature that are related to anomalies in winter monsoon strength controlled by the latitudinal migration of ITCZ. However, neither reef-water pH nor temperature can fully explain the large changes in growth rates, due to the antiphase relationship between growth rate and Ω_{cf} as well as small variations in SST at this tropical latitude. We suggest that monsoon- and seabird-derived nutrient inputs may have also played an important control on *Porites* growth. The negative influence of excess nutrients on coral growth has been a longstanding explanation for the demise of coastal coral reefs in the geological history (Cybulski et al., 2020; Hallock and Schlager, 1986). but has been broadly overlooked for open ocean coral reefs.

CRediT authorship contribution statement

Y. L. and K. Y. conceived and designed this project, S. T. and K. Y. conducted the field sampling, and Y. L., C. Y., T. W. and S. T. carried out all the measurements. Y. L. led manuscript writing with major supports from T.F.. All the authors contributed to the data interpretation and manuscript revision.

Declaration of Competing Interest

The authors declare that they have no known competing financial interests or personal relationships that could have appeared to influence the work reported in this paper.

Data availability

All data are available in the supplementary materials

Acknowledgements

This work was funded by National Natural Science Foundation of China (Grant 41922019; 42276070).

Appendix A. Supplementary data

Supplementary data to this article can be found online at https://doi.org/10.1016/j.palaeo.2023.111488.

References

Albright, R., et al., 2018. Carbon dioxide addition to coral reef waters suppresses net community calcification. Nature 555, 516–519. https://doi.org/10.1038/nature25968.

Allemand, D., Tambutté, É., Zoccola, D., Tambutté, S., 2011. Coral calcification, cells to reefs. In: Dubinsky, Z., Stambler, N. (Eds.), Coral Reefs: AnEcosystem in Transition. Springer, Dordrecht, pp. 119–150. https://doi.org/10.1007/978-94-007-0114-4_91.

Burke, L., Selig, E., Spalding, M., 2002. Reefs at Risk in Southeast Asia. World Resources Institute, Washington, DC.

Burton, E.A., Walter, L.M., 1987. Relative precipitation rates of aragonite and Mg calcite from seawater: Temperature or carbonate ion control? Geology 15, 111–114. https://doi.org/10.1130/0091-7613(1987)15<111:RPROAA>2.0.CO;2.

Cantin, N.E., Cohen, A.L., Karnauskas, K.B., Tarrant, A.M., McCorkle, D.C., 2010. Ocean warming slows coral growth in the central Red Sea. Science 329, 322–325. https://doi.org/10.1126/science.1190182.

Chen, X., et al., 2019. Atmospheric nitrogen deposition increases the possibility of macroalgal dominance on remote coral reefs. J. Geophys. Res. Biogeosci. 124, 1355–1369. https://doi.org/10.1029/2019JG005074.

Chen, X., et al., 2021. A replication study on coral δ11B and B/Ca and their variation in modern and fossil Porites: Implications for coral calcifying fluid chemistry and seawater pH changes over the last millennium. Paleoceanogr. Paleoclimatol. 36, e2021PA004319 https://doi.org/10.1029/2021PA004319.

Clark, T.R., et al., 2014a. Discerning the timing and cause of historical mortality events in modern Porites from the Great Barrier Reef. Geochim. Cosmochim. Acta 138, 57–80. https://doi.org/10.1016/J.GCA.2014.04.022.

Clark, T.R., et al., 2014b. Testing the precision and accuracy of the U-Th chronometer for dating coral mortality events in the last 100 years. Quat. Geochronol. 23, 35–45. https://doi.org/10.1016/j.quageo.2014.05.002.

Cunning, R., Baker, A.C., 2012. Excess algal symbionts increase the susceptibility of reef corals to bleaching. Nat. Clim. Chang. 3, 259–262. https://doi.org/10.1038/nclimate1711.

Cybulski, J.D., et al., 2020. Coral reef diversity losses in China's Greater Bay Area were driven by regional stressors. Sci. Adv. 6, eabb1046 https://doi.org/10.1126/sciadv.abb1046.

D'Olivo, J.P., Ellwood, G., DeCarlo, T.M., McCulloch, M.T., 2019. Deconvolving the long-term impacts of ocean acidification and warming on coral biomineralisation. Earth Planet. Sci. Lett. 526, 115785 https://doi.org/10.1016/j.epsl.2019.115785.

D'Olivo, J.P., McCulloch, M.T., Eggins, S.M., Trotter, J., 2015. Coral records of reef-water pH across the central Great Barrier Reef, Australia: assessing the influence of river runoff on inshore reefs. Biogeosciences 12, 1223–1236. https://doi.org/10.5194/bg-12-1223-2015.

De'ath, G., Lough, J.M., Fabricius, K.E., 2009. Declining coral calcification on the Great Barrier Reef. Science 323, 116–119. https://doi.org/10.1126/science.1165283.

DeCarlo, T.M., et al., 2017. Community production modulates coral reef pH and the sensitivity of ecosystem calcification to ocean acidification. J. Geophys. Res. Oceans 122, 745–761. https://doi.org/10.1002/2016JC012326.

DeCarlo, T.M., et al., 2020. Nutrient-supplying Ocean currents modulate coral bleaching susceptibility. Sci. Adv. 6, eabc5493 https://doi.org/10.1126/sciadv.abc5493.

Deng, W., et al., 2017. A comparison of the climates of the medieval climate Anomaly, Little Ice Age, and current warm period reconstructed using coral records from the northern South China Sea. J. Geophys. Res. Oceans 122, 264–275. https://doi.org/10.1002/2016JC012458.

Descolas-Gros, C., Fontugne, M., 1990. Stable carbon isotope fractionation by marine phytoplankton during photosynthesis. Plant Cell Environ. 13, 207–218. https://doi.org/10.1111/j.1365-3040.1990.tb01305.x.

Dickson, A.G., 1990. Thermodynamics of the dissociation of boric acid in synthetic seawater from 273.15 to 318.15 K. Deep Sea Res. Part I Oceanogr. Res. Pap. 37, 755–766. https://doi.org/10.1016/0198-0149(90)90004-F.

Dickson, A.G., 1990b. Standard potential of the reaction: AgCl(s) + 1/2H2 = Ag(s) + HCl(aq) and the standard acidity constant of the ion HSO4- in synthetic seawater from 273.15 to 318.15 K. J. Chem. Thermodyn. 22, 113–127. https://doi.org/10.1016/0021-9614(90)90074-Z.

Dickson, A.G., Millero, F.J., 1987. A comparison of the equilibrium constants for the dissociation of carbonic acid in seawater media. Deep Sea Res. Part I Oceanogr. Res. Pap. 34, 1733–1743. https://doi.org/10.1016/0198-0149(87)90021-5.

Foster, G.L., Pogge von Strandmann, P.A.E., Rae, J.W.B., 2010. Boron and magnesium isotopic composition of seawater. Geochem. Geophys. Geosyst. 11, Q08015. https://doi.org/10.1029/2010GC003201.

Furla, P., Galgani, I., Durand, I., Allemand, D., 2000. Sources and mechanisms of inorganic carbon transport for coral calcification and photosynthesis. J. Exp. Biol. 203, 3445–3457. https://doi.org/10.1242/jeb.203.22.3445.

Graham, N.A.J., et al., 2018. Seabirds enhance coral reef productivity and functioning in the absence of invasive rats. Nature 559, 250–253. https://doi.org/10.1038/s41586-018-0202-3.

Guillermic, M., et al., 2021. Thermal stress reduces pocilloporid coral resilience to ocean acidification by impairing control over calcifying fluid chemistry. Sci. Adv. 7, eaba9958. https://doi.org/10.1126/SCIADV.ABA9958.

Guo, W., 2019. Seawater temperature and buffering capacity modulate coral calcifying pH. Sci. Rep. 9, 1189. https://doi.org/10.1038/s41598-018-36817-y.

Hallock, P., Schlager, W., 1986. Nutrient excess and the demise of coral reefs and carbonate platforms. Palaios 1, 389–398. https://doi.org/10.2307/3514476.

Han, T., et al., 2019a. The decadal variability of the Global Monsoon links to the North Atlantic climate since 1851. Geophys. Res. Lett. 46, 9054–9063. https://doi.org/10.1029/2019GL081907.

Han, T., et al., 2019b. Links between the coral δ13C record of primary productivity variations in the northern South China Sea and the East Asian Winter Monsoon. Geophys. Res. Lett. 46, 14586–14594. https://doi.org/10.1029/2019GL085030.

Haug, G.H., Hughen, K.A., Sigman, D.M., Peterson, L.C., Röhl, U., 2001. Southward migration of the intertropical convergence zone through the Holocene. Science 293, 1304–1308. https://doi.org/10.1126/science.1059725.

Holcomb, M., DeCarlo, T.M., Gaetani, G.A., McCulloch, M., 2016. Factors affecting B/Ca ratios in synthetic aragonite. Chem. Geol. 437, 67–76. https://doi.org/10.1016/j.chemgeo.2016.05.007.

Hughes, T.P., et al., 2017. Coral reefs in the Anthropocene. Nature 546, 82–90. https://doi.org/10.1038/nature22901.
Kang, H., et al., 2021. Skeletal growth response of Porites coral to longterm ocean warming and acidification in the South China Sea. J. Geophys. Res. Biogeosci. 126, e2021JG006423 https://doi.org/10.1029/2021JG006423.
Klochko, K., Kaufman, A.J., Yao, W., Byrne, R.H., Tossell, J.A., 2006. Experimental measurement of boron isotope fractionation in seawater. Earth Planet. Sci. Lett. 248, 276–285. https://doi.org/10.1016/j.epsl.2006.05.034.
Landrum, L., et al., 2013. Last Millennium climate and its variability in CCSM4. J. Clim. 26, 1085–1111. https://doi.org/10.1175/JCLI-D-11-00326.1.
Lewis, E.R., Wallace, D.W.R., 1998. Program Developed for CO2 System Calculations. USDOE Office of Energy Research, Washington DC. https://doi.org/10.2172/63971.
Liu, K.-K., et al., 2013. Inter-annual variation of chlorophyll in the northern South China Sea observed at the SEATS Station and its asymmetric responses to climate oscillation. Biogeosciences 10, 7449–7462. https://doi.org/10.5194/bgd-10-6899-2013.
Liu, Y., et al., 2014. Acceleration of modern acidification in the South China Sea driven by anthropogenic CO2. Sci. Rep. 4, 5148. https://doi.org/10.1038/srep05148.
Lorrain, A., et al., 2017. Seabirds supply nitrogen to reef-building corals on remote Pacific islets. Sci. Rep. 7, 3721. https://doi.org/10.1038/s41598-017-03781-y.
Lough, J.M., Barnes, D.J., 1997. Several centuries of variation in skeletal extension, density and calcification in massive Porites colonies from the Great Barrier Reef: a proxy for seawater temperature and a background of variability against which to identify unnatural change. J. Exp. Mar. Biol. Ecol. 211, 29–67. https://doi.org/10.1016/S0022-0981(96)02710-4.
Mann, M.E., et al., 2009. Global signatures and dynamical origins of the little ice age and medieval climate anomaly. Science 326, 1256–1260. https://doi.org/10.1126/science.1177303.
Mass, T., et al., 2017. Amorphous calcium carbonate particles form coral skeletons. Proc. Natl. Acad. Sci. U. S. A. 114, E7670–E7678. https://doi.org/10.1073/pnas.1707890114.
Masson-Delmotte, V., et al., 2014. Information from paleoclimate archives. In: Stocker, T. F., et al. (Eds.), Climate Change 2013-the Physical Science Basis: Working Group I Contribution to the Fifth Assessment Report of the Intergovernmental Panel on Climate Change. Cambridge University, Cambridge, pp. 383–464. https://doi.org/10.1017/CBO9781107415324.013.
McConnaughey, T., 1989. 13C and 18O isotopic disequilibrium in biological carbonates: I. Patterns. Geochim. Cosmochim. Acta 53, 151–162. https://doi.org/10.1016/0016-7037(89)90282-2.
McCulloch, M.T., D'Olivo, J.P., Falter, J., Holcomb, M., Trotter, J.A., 2017. Coral calcification in a changing world and the interactive dynamics of pH and DIC upregulation. Nat. Commun. 8, 15686. https://doi.org/10.1038/ncomms15686.
McCulloch, M., Falter, J., Trotter, J., Montagna, P., 2012. Coral resilience to ocean acidification and global warming through pH up-regulation. Nat. Clim. Chang. 2, 623–627. https://doi.org/10.1038/nclimate1473.
Mehrbach, C., Culberson, C.H., Hawley, J.E., Pytkowicx, R.M., 1973. Measurement of the apparent dissociation constants of carbonic acid in seawater at atmospheric pressure. Limnol. Oceanogr. 18, 897–907. https://doi.org/10.4319/lo.1973.18.6.0897.
Mucci, A., 1983. The solubility of calcite and aragonite in seawater at various salinities, temperatures, and one atmosphere total pressure. Am. J. Sci. 283, 780–799. https://doi.org/10.2475/ajs.283.7.780.
Neukom, R., Steiger, N., Gómez-Navarro, J.J., Wang, J., Werner, J.P., 2019. Evidence for globally coherent warm and cold periods over the preindustrial Common Era. Nature 571, 550–554. https://doi.org/10.1038/s41586-019-1401-2.
Pelejero, C., et al., 2005. Preindustrial to modern interdecadal variability in coral reef pH. Science 309, 2204–2207. https://doi.org/10.1126/science.1113692.
Perry, C.T., et al., 2018. Loss of coral reef growth capacity to track future increases in sea level. Nature 558, 396–400. https://doi.org/10.1038/s41586-018-0194-z.
Ren, H., et al., 2017. 21st-century rise in anthropogenic nitrogen deposition on a remote coral reef. Science 356, 749–752. https://doi.org/10.1126/science.aal3869.
Schneider, T., Bischoff, T., Haug, G.H., 2014. Migrations and dynamics of the Intertropical Convergence Zone. Nature 513, 45–53. https://doi.org/10.1038/nature13636.
Sevilgen, D.S., et al., 2019. Full in vivo characterization of carbonate chemistry at the site of calcification in corals. Sci. Adv. 5, eaau7447 https://doi.org/10.1126/sciadv.aau7447.
Swart, P.K., et al., 2010. The 13C Suess effect in scleractinian corals mirror changes in the anthropogenic CO2 inventory of the surface oceans. Geophys. Res. Lett. 37, L05604. https://doi.org/10.1029/2009GL041397.
Thurber, R.L.V., et al., 2014. Chronic nutrient enrichment increases prevalence and severity of coral disease and bleaching. Glob. Chang. Biol. 20, 544–554. https://doi.org/10.1111/gcb.12450.
Tseng, C.-M., Wong, G.T.F., Lin, I.-I., Wu, C.-R., Liu, K.-K., 2005. A unique seasonal pattern in phytoplankton biomass in low-latitude waters in the South China Sea. Geophys. Res. Lett. 32, L08608. https://doi.org/10.1029/2004GL022111.
Wall, M., Fietzke, J., Crook, E.D., Paytan, A., 2019. Using B isotopes and B/Ca in corals from low saturation springs to constrain calcification mechanisms. Nat. Commun. 10, 3580. https://doi.org/10.1038/s41467-019-11519-9.
Wang, B.-S., et al., 2010. Direct separation of boron from Na- and Ca-rich matrices by sublimation for stable isotope measurement by MC-ICP-MS. Talanta 82, 1378–1384. https://doi.org/10.1016/j.talanta.2010.07.010.
Wei, G., McCulloch, M.T., Mortimer, G., Deng, W., Xie, L., 2009. Evidence for ocean acidification in the Great Barrier Reef of Australia. Geochim. Cosmochim. Acta 73, 2332–2346. https://doi.org/10.1016/j.gca.2009.02.009.
Wu, L., et al., 2018a. Nitrogen cycling in the soil-plant system along a series of coral islands affected by seabirds in the South China Sea. Sci. Total Environ. 627, 166–175. https://doi.org/10.1016/j.scitotenv.2018.01.213.
Wu, H.C., et al., 2018b. Surface Ocean pH variations since 1689 CE and recent ocean acidification in the tropical South Pacific. Nat. Commun. 9, 2543. https://doi.org/10.1038/s41467-018-04922-1.
Xu, L., et al., 2016. Decline of recent seabirds inferred from a composite 1000-year record of population dynamics. Sci. Rep. 6, 35191. https://doi.org/10.1038/srep35191.
Yan, H., et al., 2018. Air-sea CO2 fluxes and spatial distribution of seawater pCO2 in Yongle Atoll, northern-central South China Sea. Cont. Shelf Res. 165, 71–77. https://doi.org/10.1016/j.csr.2018.06.008.
Yan, H., et al., 2019. Regional coral growth responses to seawater warming in the South China Sea. Sci. Total Environ. 670, 595–605. https://doi.org/10.1016/j.scitotenv.2019.03.135.
Yan, H., Soon, W., Wang, Y., 2015. A composite sea surface temperature record of the northern South China Sea for the past 2500 years: a unique look into seasonality and seasonal climate changes during warm and cold periods. Earth Sci. Rev. 141, 122–135. https://doi.org/10.1016/j.earscirev.2014.12.003.
Yancheva, G., et al., 2007. Influence of the intertropical convergence zone on the East asian monsoon. Nature 445, 74–77. https://doi.org/10.1038/nature05431.
Zeebe, R.E., Sanyal, A., Ortiz, J.D., Wolf-Gladrow, D.A., 2001. A theoretical study of the kinetics of the boric acid–borate equilibrium in seawater. Mar. Chem. 73, 113–124. https://doi.org/10.1016/S0304-4203(00)00100-6.
Zhao, M., et al., 2016. The coral communities of Yongle atoll: status, threats and conservation significance for coral reefs in South China Sea. Mar. Freshw. Res. 67, 1888–1896. https://doi.org/10.1071/MF15110.
Zoccola, D., et al., 2015. Bicarbonate transporters in corals point towards a key step in the evolution of cnidarian calcification. Sci. Rep. 5, 09983. https://doi.org/10.1038/srep09983.